# Wave Overtopping of smooth impermeable seawalls under Unidirectional Bimodal Sea Conditions

Stephen Orimoloye[a], Jose Horrillo-Caraballo[a], Harshinie Karunarathna[a], Dominic E. Reeve [a]*

[a]*Energy & Environment Research Group, Zienkiewicz Centre for Computational Engineering, College of Engineering, Swansea University, Swansea, SA1 8EN, United Kingdom *Corresponding Author: d.e.reeve@swansea.ac.uk*

## Abstract

Reduction of risks due to overtopping of coastal defences is an essential requirement for the design, management and adaptation of coastal structures. Extensive knowledge is available on the prediction of overtopping of smooth, sloping and vertical impermeable seawalls. The existing prediction methods provide less certain guidance for combined wind and swell conditions. This experimental study focuses on overtopping characteristics of coastal seawalls under random bimodal waves. Both unimodal and corresponding bimodal conditions were simulated under different slopes and crest freeboards. Proportions of swell in the bimodal sea were varied in each test. Mean wave overtopping discharges were calculated for non-breaking random waves over at least 1000 waves. EurOtop formulae agree closely with our measurements from the unimodal experiments whereas they underpredict the observed wave overtopping rates for bimodal conditions even when using the recommended $T_{m-1,0}$ period for such cases. A modification to the EurOtop formula is proposed on the basis of the experimental results, to better capture the overtopping discharge under bimodal conditions.

*Keywords:* bimodal waves, wave overtopping, EurOtop, swell, storms, seawalls

## 1. Introduction

Prediction of wave overtopping is a crucial component of coastal structure and seawall design. Sea states are generally irregular, being composed of a combination of harmonics with varying frequencies and directions, especially for shorelines exposed to very large fetches. These locations are influenced predominantly by both wind and swell waves, and the energy characteristics can be bimodal (Rychlik et al., 1997).

Individually, wind sea and swell are characterised by a unimodal frequency spectrum, (i.e. one spectral peak). Similarly, the directional distribution of energy across a sea state is also characterised by a unimodal spreading function, (e.g. Goda 2010, Reeve et al 2015). Such a picture is useful in locations exposed to short fetches. For the case of shorelines exposed to long fetches, bimodal or multi-modal distributions of energy can be encountered. The simplest case is bimodality. This can occur in the frequency spectrum through the superposition of wind sea and swell components; and also in the directional distribution of waves, especially when

the swell has been generated by a distant storm with different directional properties to the local prevailing wind sea.

Evidently, attempting to create a sea state that exhibits both frequency and directional bimodality in a laboratory setting is challenging. A simpler case that can be achieved in a wave flume is a bimodal frequency spectrum. Some results of wave overtopping under this type of condition, (e.g. Hawkes et al 1998, Hedges & Shareef 2002, Kashima et al. 2010), have suggested that overtopping can be enhanced relative to predictions based on unimodal wave conditions; and might be expected to be representative of combined wind and swell conditions with a narrow directional spread. A relatively recent and well-documented example of this situation was the period during the boreal winter of 2013/2014 in which a rapid succession of storms tracked across the N. Atlantic from the USA to NW Europe with very similar tracks. This resulted in superimposed swell and wind seas with very similar directional characteristics, which led to widespread coastal flooding and damage to sea defences on the west and southwest coasts of the UK, (see e.g. Thompson et al., 2017 and references therein). Here, we focus on bimodality in the frequency spectrum but note in passing that van der Werf & Van Ghent (2018) investigated overtopping under bimodal seas and found that the presence of swells with low steepness enhanced wave overtopping with obliquely intersecting wind and swell waves.

The effects of swell have been characterised by swell percentage, (see Hawkes et al., 1998; Ewans et al., 2006) and also by the peak frequency of swell waves present in the sea state, (Hedges & Shareef, 2002). In most cases, a complete partitioning of irregular waves into swell and wind seas would be necessary to determine the percentage of swell, (Hanson and Phillips, 2001).

Physical modelling techniques have been applied extensively to investigate wave-structure interactions and wave overtopping of coastal structures under unimodal sea conditions, (e.g. Owen, 1982; Franco et al., 1994). These studies have been the basis for guidance wave overtopping estimates of coastal defences. De Rouck et al., (2009) provided an expanded summary of wave overtopping datasets compiled from numerous physical experiments covering various seawall geometries. More details of these studies can be found in (Troch et al., 2004; De Rouck et al., 2009; Franco et al., 1994). These databases have been presented by van der Meer et al., (2005, 2009) and Pullen et al., (2007) – henceforth referred to as EurOtop 2007.

A series of wave overtopping tests presented in Gallach Sanchez et al. (2016) and Victor and Troch (2012) focussed primarily on steep low-crested coastal seawalls in deep and shallow water conditions. Based on these studies, and many more, some significant modifications to wave overtopping formulations have been made (van der Meer and Bruce, 2013; van der Meer et al., 2018 – henceforth referred to as EurOtop 2018). Concerning wave overtopping estimates for bimodal seas the use of $T_{m-1,0}$, which weights the wave period towards larger values, has been

proposed by van Gent (1999, 2001, 2002) and has been included in the EurOtop (2018) guidance.

The present study aims to understand better the wave overtopping characteristics of coastal seawalls by normally incident unidirectional bimodal wave conditions. Commonly, bimodal sea conditions containing swell have been constructed from the superposition of two JONSWAP spectra; one representing the wind sea and one the swell. With this construction, there will be a degree of overlap between the spectra and a sharp break between the swell and wind sea as a separation frequency is not present. It contrasts with the practice-based approach in which the swell and wind-sea components have no overlap (Bradbury et al., 2007). Here, we use the former method to create a set of bimodal sea states that have varying proportions of swell, while at the same time containing a fixed amount of energy. We refer to a set of sea states that have a fixed amount of energy but varying proportions of swell and wind sea as 'energy conserved' bimodal waves. The advantage of this method is that it allows us to relate overtopping to the total energy of the sea state. The extremes of these conditions are 'pure wind sea' at one end and 'pure swell' at the other; with both cases resulting in a unimodal spectrum. The details of generating such sea states may be found in Orimoloye et al. (2019a) and are presented in outline only in this paper. Here, we investigate whether the distribution of wave energy across swell and wind wave components has a quantifiable effect on mean wave overtopping rates. The paper is divided into 6 sections, the following section (Section 2) focuses on the state of art of wave overtopping prediction formulations. Sections 3 and 4 describe the prescribed bimodal sea conditions and experimental tests, respectively. Results and discussions are presented in Section 5 while Section 6 concludes the paper.

## 2. State of the art

Comprehensive histories of research into wave overtopping of impermeable coastal seawalls may be found in Hedges and Reis (1998), and Burcharth and Hughes (2002). According to several previous studies (e.g. Burcharth and Andersen, 2007; Franco et al., 2009; and EurOtop 2018) and as illustrated in Fig. (1), random waves (expressed spectrally in terms of $H_{m0}$, $T_{m-1,0}$) would generally overtop a sloping impermeable structure whenever the wave run-up exceeds the crest freeboard $R_c$.

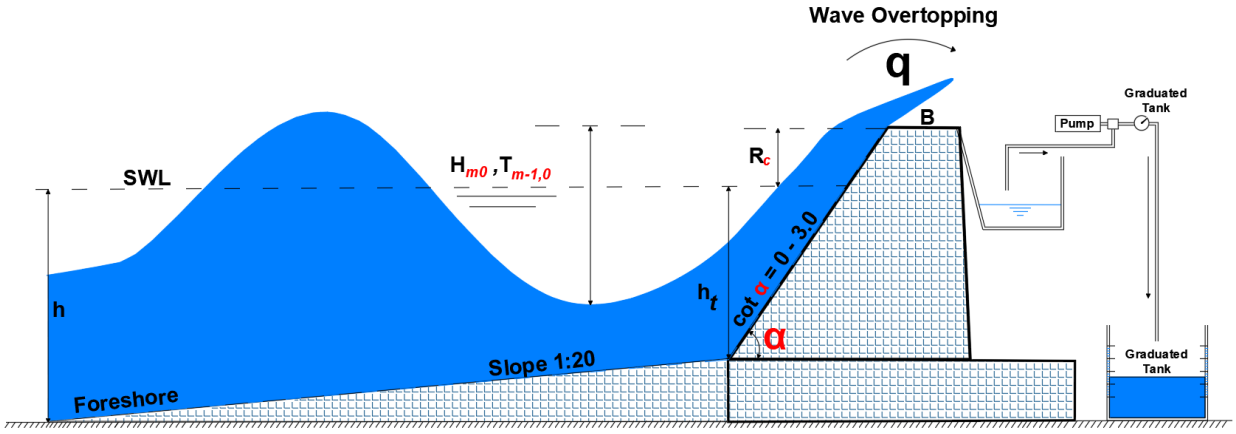


Fig. 1: *A schematic representation of wave overtopping of a sloping seawall*

As the waves are random the overtopping will vary from wave to wave. Owen (1980) denoted the mean overtopping rate, averaged over many waves, by $Q_m$ and proposed a negative exponential relationship between $Q_m$ and the crest freeboard $R_c$. Eq. (1) shows the mathematical representation as:

$$Q_m = Q^* T_m g H_s \qquad (1)$$

where

$$Q^* = Ae^{-\frac{BR^*}{r}}, \qquad and \qquad R^* = \frac{R_c}{T_m\sqrt{gH_s}}$$

or, equivalently,

$$Q_m = gH_s T_m Ae^{-\frac{BR_c}{rT_m\sqrt{gH_s}}}.$$

In this equation, $H_s$ represents the significant wave height at the toe of the structure, A and B are empirically fitted coefficients that are dependent upon the seawall geometry, and $r$ is a roughness factor. Since Owen's first formulation, several definitions have been given to coefficients $A$ and $B$ as additional experimental results became available. Further, the entire relationship between wave overtopping and the crest freeboard has been redefined by different authors. These refinements have been made to accommodate several other influence factors such as the presence of berms $\gamma_b$, permeability and roughness $\gamma_f$, for oblique wave attack, $\gamma_\beta$, influence factor by a vertical wall $\gamma_v$ and for different geometries $\gamma_*$. A summary of wave overtopping formulae have been presented by (Hedges and Reis, 1998; Burcharth and Hughes, 2002) and these are used as the basis of the extended tabulation in Table 1. In many of

the original papers mean overtopping discharge has been denoted by $q$ and we adopt this notation for the remainder of the paper. One of the most significant definitions of wave overtopping formulae was summarized in Pullen et al. (2007), based on TAW (2002), and included the following formula for breaking and non-breaking waves:

$$\frac{q}{\sqrt{gH_{m0}^3}} = \frac{0.067}{\sqrt{tan \propto}} . \gamma_b . \xi_{m-1,0} \; exp\left(-4 \cdot 75 \frac{R_c}{\xi_{m-1,0} . H_{m0} . \gamma_b . \gamma_f . \gamma_\beta . \gamma_v}\right) \tag{2a}$$

with a maximum occurring during a non-breaking wave as:

$$\frac{q}{\sqrt{gH_{m0}^3}} = 0.2 \, exp\left(-2 \cdot 6 \frac{R_c}{H_{m0} . \gamma_f . \gamma_\beta}\right) \tag{2b}$$

Victor and Troch (2012) and van der Meer and Bruce (2013) propose an alternative overtopping formulation which includes low crested freeboards. Modifications based on varieties of smooth slopes led to the following formulae for non-breaking wave conditions:

$$\frac{q}{\sqrt{gH_{m0}^3}} = A \, exp\left(-B \frac{R_c}{H_{m0}}\right)^C \tag{3}$$

Current guidance in EurOtop 2018 advises that coefficients $A$ and $B$ for non-breaking waves across different slopes are defined by:

$$A = \begin{cases} 0.09 - 0.01(2 - \cot\alpha)^{2.1} & for \cot\alpha \le 2 \\ 0.09 & for \cot\alpha \ge 2 \end{cases} \tag{4}$$

and:

$$B = \begin{cases} 1.5 + 0.42(2 - \cot\alpha)^{1.5} \quad (with \, a \, maximum \, of \; 2.35) & for \cot\alpha \le 2 \\ 1.5 & for \cot\alpha \ge 2 \end{cases} \tag{5}$$

The coefficient C in Equation (3) is set to 1.3 in the EurOtop 2007 and 2018 formulations, whereas earlier approaches have used a value of 1.0. The optimum value of C is the subject of ongoing discussion, (see e.g. Van der Werf and Van Gent, 2018; Van Gent and Van der Werf, 2019; Chen et al., 2020). The empirical models described above apply for steep slopes up to vertical walls, (as defined in Eqs (4 & 5), and provide an efficient means to predict overtopping rates based on specific structure geometries and wave conditions. In what follows we focus discussion of our results with the EurOtop 2018 formulae, a widely-used practitioners' guide that supersedes EurOtop 2007.

An alternative to empirical formulae is neural network models, (NN). These require training on large datasets, which has been feasible with the development of the CLASH database (De Rouck et al., 2009), and provide a non-parameteric regression model which may be interrogated across the domain defined by the training data. One such NN is that developed by Delft Hydraulics, (DHNN), which is described in van Gent et al., (2007), and is used later in this paper in comparisons with our experimental results.

Table 1: Design formulations on dimensionless discharge, dimensionless freeboard and overtopping model (modified from Hedges and Reis, 1998; Burcharth and Hughes, 2002).

| Reference | Dimensionless discharge $Q^*$ | Dimensionless Freeboard $R^*$ | Overtopping model | Applicability |
|---|---|---|---|---|
| Owen (1980) | $\frac{q}{gH_sT_m}$ | $\frac{R_c}{T_m\sqrt{gH_s}}$ | $Q^* = Aexp(-BR^*)$ | Impermeable smooth, rough, straight and bermed slopes |
| Bradbury et al. (1988) | $\frac{q}{gH_sT_m}$ | $\frac{R_c^2}{T_m\sqrt{gH_s^3}}$ | $Q^* = A\,(R^*)^{-B}$ | Rock armoured impermeable slopes with crown walls |
| Aminti and Franco (1988) | $\frac{q}{gH_sT_m}$ | $\frac{R_c}{H_s}$ | $Q^* = A(R^*)^{-B}$ | Rock, cube, tetrapod, double layered armoured impermeable slopes with crown walls |
| Ahrens and Heimbaugh (1988) | $\frac{q}{\sqrt{gH_s^3}}$ | $\frac{R_c}{H_sL_{0p}^{1/3}}$ | $Q^* = Aexp(-BR^*)$ | Different seawall designs |
| Pedersen and Burcharth (1993) | $\frac{qT_{0m}}{L_{0m}^2}$ | $\frac{R_c}{H_s}$ | $Q^* = AR^*$ | Rock armoured impermeable slopes with crown walls |
| De Waal and Van der Meer (1993) | $\frac{q}{\sqrt{gH_s^3}}$ | $\frac{R_c - R_{2\%}}{H_s}$ | $Q^* = Aexp(-BR^*)$ | Impermeable smooth, rough, straight and bermed slopes |
| Van der Meer (1993) | $\frac{q}{gH_sT_m}$ | $\frac{R_c}{T_m\sqrt{gH_s}}$ | $Q^* = Aexp(-BR^*)$ | Impermeable smooth, rough, straight and bermed slopes |
| Franco et al. (1994) | $\frac{q}{\sqrt{gH_s^2}}$ | $\frac{R_c}{gH_s}\frac{1}{\gamma}$ | $Q^* = Aexp(-BR^*)$ | Vertical wall breakwaters with/without perforated front wall |
| Smith et al. (1995); Van der Meer (1993, 1995) | $\frac{q}{\sqrt{gH_s^3}}\frac{tan\alpha}{\xi_{0p}}$ $for\ \xi_{0p} < 2$; $\frac{q}{\sqrt{gH_s^3}}$ $for\ \xi_{0p} > 2$ | $\frac{R_c}{H_s}\frac{tan\alpha}{\xi_{0p}}\cdot\frac{1}{\gamma}\xi_{0p} < 2$; $\frac{R_c}{H_s}\cdot\frac{1}{\gamma}$ $for\ \xi_{0p} > 2$ | $Q^* = Aexp(-BR^*)$ | Impermeable smooth, rough, straight and bermed slopes |
| Hedges and Reis (1998) | $\frac{q}{gR_{Umax}^3}$ | $\frac{R_c}{R_u max}$ | $Q^* = A(1-R_c)^B$ $for\ 0 \le R_c \le 1$; $Q = 0\ for\ R \ge 1$ | Impermeable smooth, rough, straight and bermed slopes |
| Van Gent and Smith (1999) | $\frac{q}{\sqrt{gH_{m0}^3}}$ | $\frac{R_c}{H_{m0}\xi_{m-1,0}}$ | $Q^* = Aexp(-BR^*)$ | Shallow and very shallow foreshore slopes |
| Pullen et al. (2007) | $\frac{q}{\sqrt{gH_{m0}^3}}$ | $\frac{R_c}{H_{m0}}$ | $Q^* = Aexp(-BR^*)$ | Different seawalls designs including armoured rubble mounds and composite structures |
| Altomare et al. (2016) | $\frac{q}{\sqrt{gH_{m0}^3}}$ | $\frac{R_c}{H_{m0}.(0.33+0.022.\xi_{m-1,0})}$ | $Q^* = Aexp(-BR^*)$ | Shallow and very shallow foreshore slopes |
| Van der Meer et al. (2018) | $\frac{q}{\sqrt{gH_{m0}^3}}$ | $\frac{R_c}{H_{m0}\xi_{m-1,0}\cdot\gamma_\tau}$ $for\ breaking\ waves$; $\frac{R_c}{H_{m0}}$ $for\ non-breaking\ waves$ | $Q^* = Aexp(-BR^*)$ | Different seawalls and slope designs including armoured rubble mounds and composite structures |
| Van der Werf and Van Gent (2018) | $\frac{q}{\sqrt{gH_{m0}^3}}$ | $\frac{R_c - 0.5H_{m0swell}}{H_{m0}\xi_{m-1,0}\cdot\gamma_\tau}$ $for\ breaking\ waves$; $\frac{R_c - 0.5H_{m0swell}}{H_{m0}}$ $under\ non-breaking\ waves$ | $Q^* = Aexp(-BR^*)$ | Smooth impermeable sloping dike under oblique wind and swell waves |

## 3. Test programme

### 3.1 Development of bimodal spectrum

For the purpose of this experiment, an energy-conserved bimodal spectrum was created using a four-parameter analytical approach proposed by Guedes Soares (1984). A direct superposition of the arithmetical combination of double modified JONSWAP by Hasselmann et al. (1973) were formed by using Eq. (6-10). Further details can be found in Goda (2010). For example, by superposition, the bimodal spectrum $S_{bim}$, can be expressed mathematically in terms of the wind component $S_{ww}$ and the swell component $S_{ss}$ according to Eq. (6):

$$S_{bim} = S_{ww} + S_{ss} \tag{6}$$

The combination of two different frequencies for wind-sea *i*, the swell-sea *j* components would produce the combined energy of the bimodal spectrum:

$$S(f)_{ij} = S(f)_i + S(f)_j \tag{7}$$

Applying the equation presented by Goda (2010) for separate wind and swell sea states we have:

$$S(f)_i = \beta_e H_s^2 T_i^{-4} f_i^{-5} exp[-1.25(T_i f_i)^{-4}] \gamma_i \, exp[-(T_i f_i - 1)^2 / 2\sigma^2] \tag{8}$$

$$S(f)_j = \beta_e H_s^2 T_j^{-4} f_j^{-5} exp[-1.25(T_j f_j)^{-4}] \gamma_j \, exp[-(T_j f_j - 1)^2 / 2\sigma^2] \tag{9}$$

With

$$\beta_e = \frac{0.0624}{0.230 + 0.0336\gamma_{ij} - 0.185(1.094 - 0.01915 \ln \gamma_{ij})} \left(1.094 - 0.01915 \ln \gamma_{ij}\right) \tag{10}$$

where, in Eqs. (8–10) above, $H_s$ represents the significant wave height, $T_{ij}$ the peak period, and $\gamma_{ij}$ is the peak enhancement factor of the spectrum with *i*, and *j* representing the equivalent wind and swell sea components respectively. σ is sigma defining the frequency ranges of the spectra widths $\sigma_a$ to the left and $\sigma_b$ to the right of the peak frequency f. This can be expressed as:

$$\sigma = \begin{cases} \sigma_a: \text{ 0.07 for } f \le f_i \text{ or } f_j \\ \sigma_b: \text{ 0.09 for } f \le f_i \text{ or } f_j \end{cases}$$

The constraint added in this study is that the overall energy in the bimodal spectrum was maintained as a constant value. That is, the energy of the sea state is conserved as the shape of the spectrum is varied. The $n^{th}$ moment $m_n$ of the wave spectrum is defined as:

$$m_n = \int_0^\infty f^n S(f) df \qquad (11)$$

In Eq. (11), *n* is the order of the spectral moment. For example, for a given sea state, the total spectral energy $m_0$ can be determined using Eq. (11). A specific percentage of swell $S_0$ can be introduced into the bimodal spectrum using Eq. (11-12) by sharing the total energy between the wind-sea and the swell. The corresponding wave heights for the wind sea, swell and combined sea state are given by:

$$H_{m0W} = 4 * \sqrt{(1 - S_0 * m_0)}; \quad \textit{and for swell, } H_{m0S} = 4 * \sqrt{(S_0 * m_0)} \qquad (12)$$

$$H_{m0} = \sqrt{H_{m0S}^2 + H_{m0W}^2} \qquad (13)$$

Full details of the methodology may be found in Orimoloye et al. (2019a). Fig. 2 shows examples of the energy conserved bimodal spectra using different $S_0$ and peak periods, while keeping the overall energy content the same.

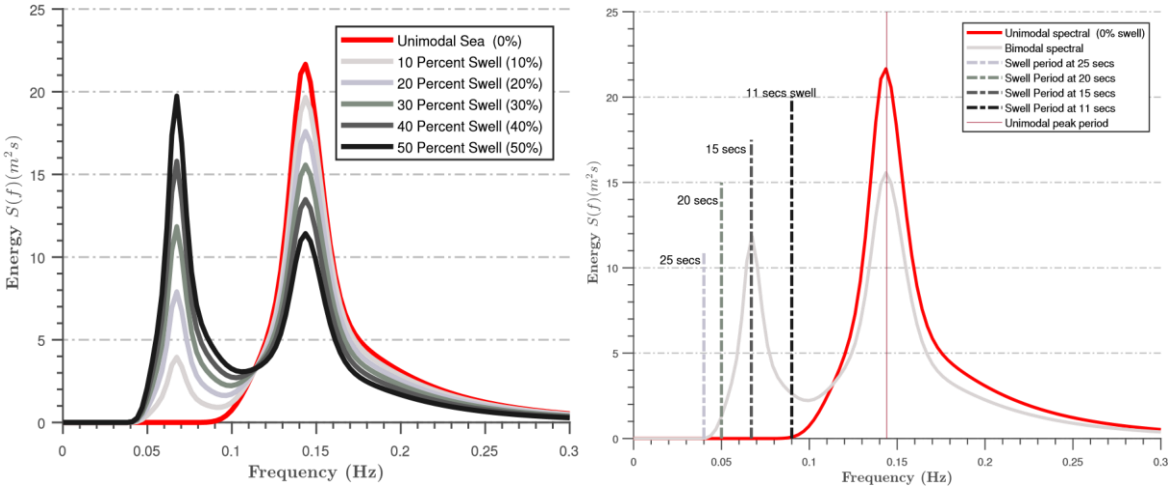


(a) (b)

Fig. 2: *(a) An example of the bimodal spectra with different swell percentages for swell peak periods of 15 secs (b) Shifting patterns of swell peak periods from 11-25 secs Orimoloye et al. (2019a).*

3.2 Tested wave cases

In Fig. (2), the unimodal sea state is a simple wind sea configuration with a unimodal spectrum (shown in red). Different bimodal spectra with the same energy were then developed by introducing different swell components of different percentages at different frequencies, as shown in Fig. 2(b). Table 2 contains the ranges of parameters tested in this study. Different spectral components ($H_{m0,}$ $T_{Wm-1,0}$, and $T_{Sm-1,0}$ ) each for wind and swell seas were selected within the ranges shown in the Table.

Table 2: An example of 13 different wave conditions generated from the same-energy sea state with *wave height* of 4 metres and wind wave period of 7 secs.

| ID | Test-No | $T_{pW}$ (secs) | $T_{pS}$ (secs) | Swell (%) | Mode (Unimodal = 1 Bimodal = 2 ) |
|---|---|---|---|---|---|
| 1 | T001-1 | 7 | 11 | 25 | 2 |
| 2 | T001-2 | 7 | 15 | 25 | 2 |
| 3 | T001-3 | 7 | 20 | 25 | 2 |
| 4 | T001-4 | 7 | 25 | 25 | 2 |
| 5 | T001-5 | 7 | 11 | 50 | 2 |
| 6 | T001-6 | 7 | 15 | 50 | 2 |
| 7 | T001-7 | 7 | 20 | 50 | 2 |
| 8 | T001-8 | 7 | 25 | 50 | 2 |
| 9 | T001-9 | 7 | 11 | 75 | 2 |
| 10 | T001-10 | 7 | 15 | 75 | 2 |
| 11 | T001-11 | 7 | 20 | 75 | 2 |
| 12 | T001-12 | 7 | 25 | 75 | 2 |
| 13 | T001-13 | 7 | N/A | 0 | 1 |

The purpose of present study is to examine bimodal overtopping induced by non-breaking wave conditions; hence datasets are chosen firstly to avoid effects of depth-induced wave breaking conditions. The prototype scale is based on the wave climate around the Welsh coastline with wave heights ranging from 2 metres to 5 metres, (corresponding to a range of 0.05 to 0.125 metres at Froude's scaling of 1:40). Three water depths of 0.60 m, 0.65 m and 0.70 are chosen at the flat and deeper part of the flume. The corresponding water depths at the toe of the structure were 0.49 m, 0.54 m, 0.59 m respectively. The three crest freeboards that were used in this study correspond to the three different water depths. Representative values of $H_{m0}$ and $T_{m-1,0}$ were derived from offshore wave measurements available from national observatories. Four values of $H_{m0}$ were selected to cover a wide range of dimensionless cases of $R_c/H_{m0}$, while remaining within the capabilities of the wave maker. These were 0.05 m, 0.075 m, 0.10 m, and 0.125 m respectively. Also, the analysis of the swell percentages of the waves around the Welsh coastline revealed that a large swell percentage is possible. We designed experiments to cover the unimodal sea cases, (with 0% swell), and bimodal cases with 25%, 50%, and 75% swell, occurring at a range of different spectral peaks. The wind-wave component, with spectral peak period $T_{Wm-1,0}$ varying from 1.106 secs to 1.581 seconds, was combined with a swell wave component with corresponding spectral peak period $T_{Sm-1,0}$. Four different swell peak periods were used: 1.739, 2.372, 3.162 and 3.953 seconds which are equivalent to 11, 15, 20 and 25 seconds at prototype scale. Four values of swell percentage, $S_0$, (0, 25, 50 and 75%), were investigated. Table 3 gives further information on the test cases.

There are, therefore 13 different spectra, (including the unimodal one), for each case. As seen from Table 3, a broad range of wave steepness, $S_{m-1,0}$, (ranging from 0.01 to 0.07) was achieved in the set of experiments. In this study, a total of 24 unimodal sea states have been tested, each with different swell components in terms of peak periods and percentages. For each unimodal test, the bimodal spectra were formed by introducing 4 swell peak periods (11, 15, 20, and 25 seconds), and also 3 sets of $S_0$ (25, 50, and 75 percentages). Altogether, we have 13 tests for each unimodal case.

For example, Table 2 shows a single sea state of 4 metres wave height and 7 seconds wind peak period. The wind wave is kept fixed at 7 seconds while the swell periods and percentages are changed, (Fig. 2b), to form a complete set of 13 test conditions from this single sea condition. Altogether, from 24 different wind-sea states, a total possibility of 312 wave conditions were tested for each slope and different water depths. From these numerous sets of criteria, an optimal set of 823 datasets were chosen to accommodate reasonable range of $R_c/H_{m0}$ within a reasonable spread of results. Further details of the selection criteria are provided in the accompanying method paper.

As clearly presented in this table, the presence of swell in a single sea implementing different percentages and periods of swell in the sea states yields different spectra and of course time series with the same energy content. Details of varying wind wave spectra that were combined with their equivalent swell periods and percentages are detailed Table 3. Datasets in Table 3 are based on a Froude's scaling of 1:40 for all test cases. A full description of how the range of parameters are derived may be found in the accompanying method paper (see, Orimoloye et al., 2020b)

Table 3: Ranges of Parameters tested.

| Parameter (unit) | Range |
|---|---|
| Spectral wave height $H_{m0}$ (m) | 0.05, 0.075, 0.10, 0.125 |
| Spectral wind-wave peak period $T_{Wm-1,0}$ (s) | 1.106, 1.265, 1.423, 1.581 |
| Spectral swell-wave peak period $T_{Sm-1,0}$ (s) | 1.739, 2.371, 3.1622, 3.952 |
| Swell percentage $S_0$ | 0, 25, 50, 75 |
| Crest freeboard $R_c$ (m) | 0.1, 0.15, 0.2 |
| Water depth at wave maker h (m) | 0.60, 0.65, 0.70 |
| Water depth at structure toe $h_{toe}$ (m) | 0.49, 0.54, 0.59 |
| $\xi_{m-1,0}$ | 2.4 - 5.5 |
| Relative freeboard $R_c/H_{m0}$ | 0.8 - 4 |
| Wave steepness $S_{m-1,0}$ | 0.01 - 0.07 |
| cot $\alpha$ (–) | 0, 1.5, 3.0 |
| Slope angle (°) | 90, 33.70 and 18.43 |
| Total number of successful tests | 823 |

## 4. Laboratory experiments

The Coastal Laboratory wave flume at Swansea University consists of an Armfield wave flume 30 metres in length, 0.8 metres in width and 1.2 metres in depth respectively. Waves are generated with a HR Wallingford computer-controlled piston paddle which has the capability to reproduce user-defined spectra of different types to generate 1st order irregular waves; includes a second-order wave correction due to Schaeffer (1996); and is also equipped with an active wave absorption system to minimize the wave reflection from the wave board.

To represent a more realistic bathymetry for the experiment, the seabed was modified to a slope of 1:20 and the seawall positioned to accommodate large number of wavelengths to allow proper development of the random wave train (Fig. 3). This also gave room for a deeper surface at the wavemaker than at the structure-toe. The model is constructed with stainless steel with adjustable edges to facilitate easy reformation into other geometries. A constant crest width of 0.40 m was tested in all the experiments. The bimodal spectra, (from Section 3), were input into the wave generator in a user defined format to generate bimodal waves in random mode. As recommended by EurOtop (2018), a minimum of 1000 waves were tested for each wave conditions.

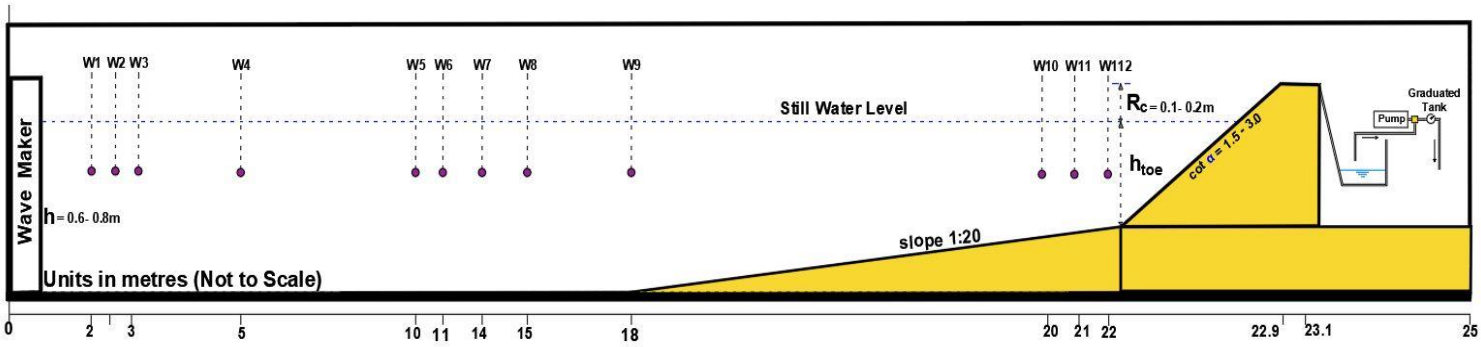


Fig. 3: *Sketch of the model set up that was applied during this experimental study.*

The wave gauges were calibrated before each test, using the calibration routine of the HR Daq system. Calibration was accepted once the correlation factor was 99.9% or better. Overtopping volumes were collected using a chute fitted directly on top of the structures placed at the rear end of the crest (Fig. 1). The chute emptied the water into the overtopping collection tank using a simple pumping system, (see, for example, Kortenhaus et al., 2004; Troch et al., 2004). The overtopping volume was obtained by measuring the water level in the calibrated tank before and after each test. To avoid changes in mean water depth the water was pumped back into the flume. The accuracy of this technique was checked by conducting repeatability tests and coefficient of variation

between repeated tests. This technique produced acceptable accuracy. In all tests considered, as expected, a higher coefficient of variation was observed in overtopping rates than wave heights. More details of these tests can be found in Orimoloye et al. (2019b &c).

In order to obtain the dimensionless wave overtopping, $H_{m0Toe}$ is required. It is determined by applying the bulk reflection coefficient obtained from the reflection analysis. The reflection analysis of acquired signals was performed using the reflection module incorporated with the HR-Daq data acquisition and processing software. This package separates reflected waves from the total signals using the method Zelt & Skjelbreia (1992) with four wave gauges. The method is an extension of the three-wave gauges least-squares solution of reflection analysis first introduced by Mansard & Funke (1980). In this experiment, the reflection analysis of wave signals was analysed using four wave gauges that are placed at the flat and deeper end of the flume are used for the reflection analysis. These wave gauges are WG5, WG6, WG7, and WG8 (Fig. 3a). The waves gauges are positioned to satisfy the requirements specified in Zelt and Skjelbreia (1992). Separation distances between the gauges were computed using offshore based linear wavelength $L_{m-1,0}$ of the incident waves, and can be expressed as $X_1 = 0$, $X_{12} = L/10$, $X_{13} = L/4$, $X_{14} = L/3$. During these tests, the wave gauges are fixed at distances 10 metres, 10.33 metres, 10.83 metres and 11.1 metres from the wave maker to satisfy the normalised denominator criteria of the HR-Daq reflection analysis module. The wave signals were analysed using Fast Fourier Transform (FFT) into frequency components in the frequency domain. Some portions of wave elevation at earlier and later parts of each simulation were ignored to allow for consistency of wave elevations. The maximum length of discarded portions were 60 seconds at the beginning and 120 seconds at the end. Bandpass filtering was applied to isolate the frequency band of $0.33f_p \leq f_p \leq 3f_p$. For the reflection analysis, The HR Merlin software (Clarke, 2010 & Mason et al., 2010) was employed. The HR Merlin software has the capability of computing different wave characteristics including the spectral incident wave height, the reflection coefficients, and the accuracy of the processes. The wave gauges were positioned not only to satisfy the limits of the wavelengths, but also to capture the reflections generated by the seawall. The output of the reflection analysis is the bimodal spectrum which can be compared to the target spectrum directly. The acceptance of the position of the wave gauges are determined using the accuracy obtained in the wave software. In the present study only non-breaking waves are tested. In this way, effects of non-linear transformations due to steepness induced wave breaking are minimal. Wave gauge positions were calibrated iteratively until optimal positions were achieved. Further details of the reflection analysis can be found in Orimoloye et al., (2020a).

In this study, three levels of the crest freeboard were tested at 0.1 metres, 0.15 metres and 0.20 metres for seawalls with slopes of 1:1.5, 1:3 and vertical seawalls. All results are for non-breaking conditions. To minimise the effects of seiche-type oscillations the active wave absorption mechanism was used to assist in damping water motions in the flume so that each run began with quiescent conditions.

## 5. **Results and Discussions**

### 5.1 Laboratory test results

Figs. (4a-d) show examples of comparisons between the target (in red dashed line) and the reproduced (with black markers) incident bimodal spectra at the structure toe, (WG12), after reflection analysis has been carried out. Overall agreement is good. The frequencies of the modal values are well captured but the peak spectral values are slightly underpredicted, an outcome of the limitations imposed by scaling and of the wave maker. The result of the spectral analysis shows that no artificial peaks are forming due to resonance effects occurring at any seiche-type frequencies. For some of the cases with the largest amounts of swell the presence of long waves was detectable at extremely low energy levels, (see Figs. 4c & d).

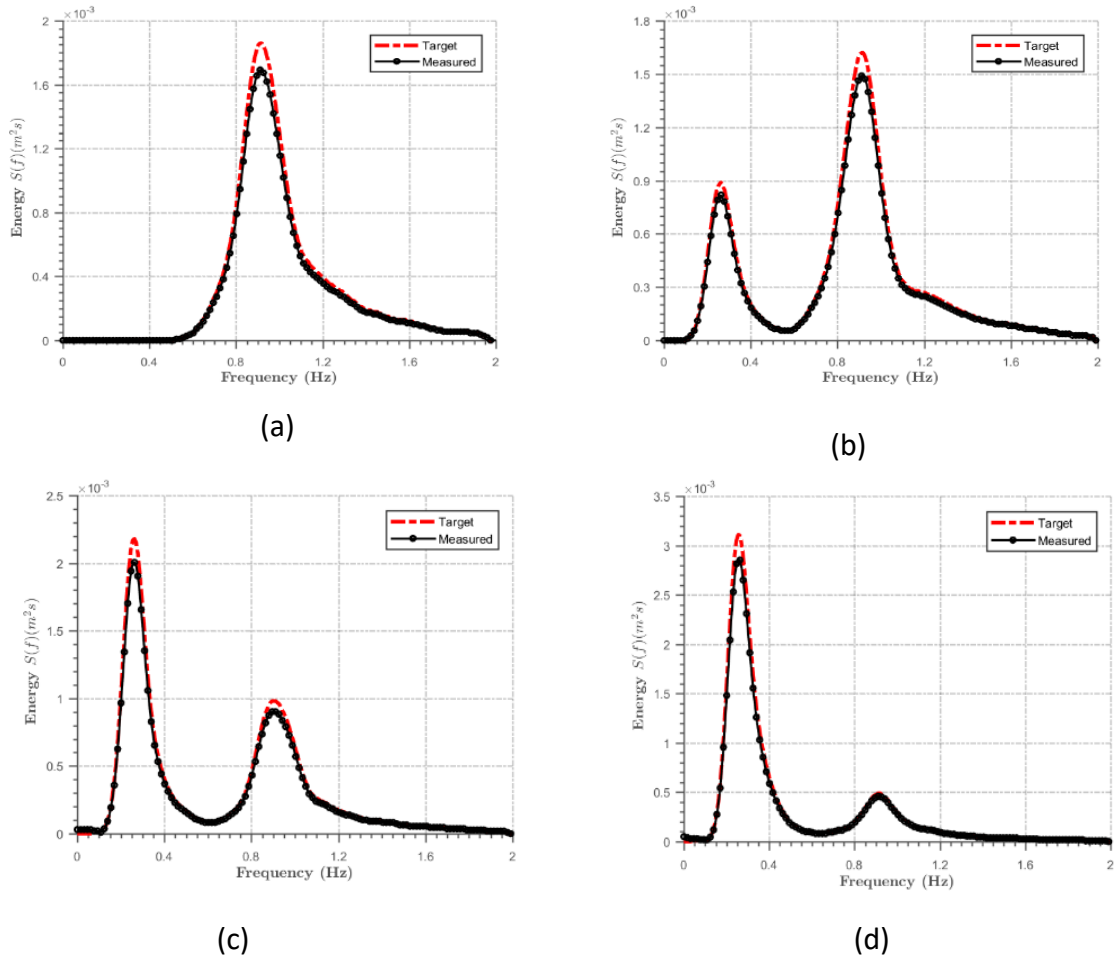


Fig. 4: *Comparison between the target bimodal spectrum (in dashed lines) and measured (with markers) for (a.) unimodal wind-sea with 0 percent swell and, (b.) 25 percent swell, (c.) 50 percent swell, and (d.) 75 percent swell.*

*5.2 Bimodal wave overtopping of sloping Seawalls*

Figs. (5 and 6) show the combination of all results of wave overtopping due to non-breaking waves obtained during this study for sloping seawalls. These estimates are derived using the overtopping formulae from EurOtop 2007 & 2018 and the DHNN model. In the case of the EurOtop 2018 model, coefficients A and B applied in Eqs. (3 to 5) also change with individual slopes using Eqs. (6 & 7) for the non-breaking wave cases. The DHNN model was used to provide an additional test against the unimodal results and was run using 15 input parameters (3 for wave conditions, and 12 for geometrical parameters), and the equivalent wave overtopping was obtained from the model by a direct first estimation.

The overtopping and corresponding 90 % confidence limits using the EurOtop 2018 method for both unimodal and bimodal cases are presented in each plot. Fig. (5) represents a gentle seawall slope (cot $\alpha$ = 3.0), and Fig. (6), a steeper seawall slope (cot $\alpha$ = 1.5). Coefficients A and B, corresponding to individual slopes, were obtained from Eqs. (3-4). Also shown are the corresponding confidence limits.

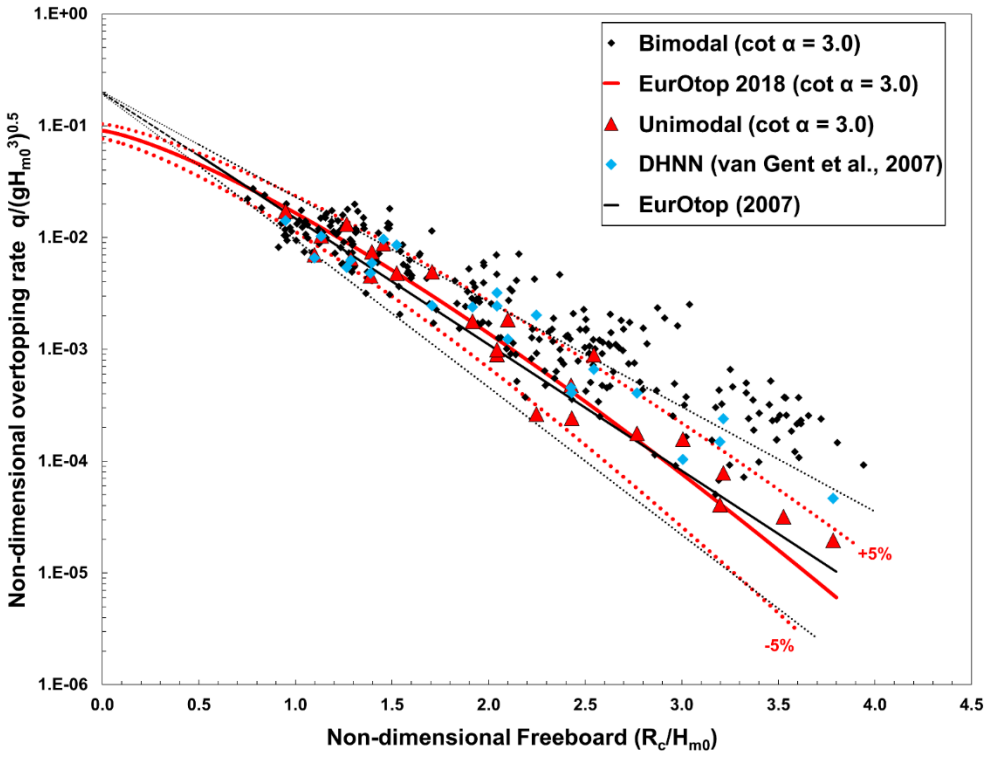


Fig. 5*: Results of non-dimensional overtopping rate against non-dimensional crest freeboard plotted for a sloping seawall with cot α = 3.0.*

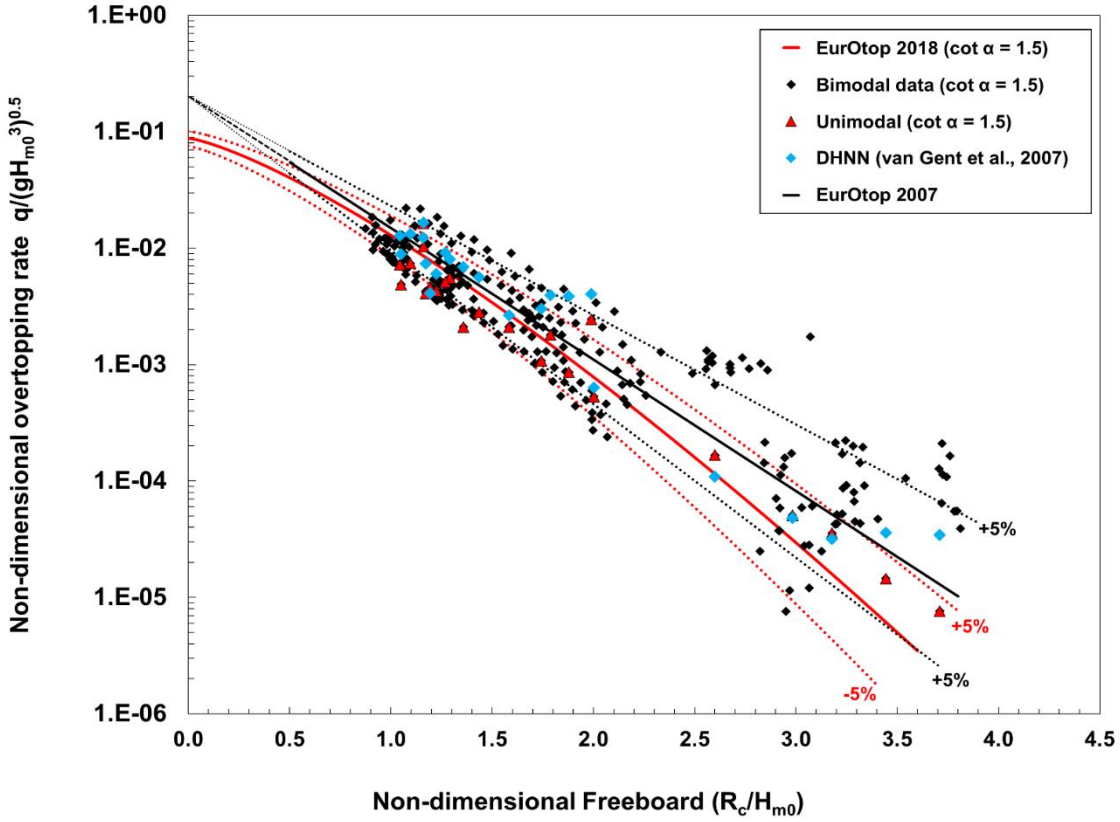


Fig. 6: *Results of non-dimensional overtopping rate against non-dimensional crest freeboard plotted for a sloping seawall with cot* $\alpha$ =1.5

Our first observation is that the majority of our overtopping results for unimodal cases fit very well within the prediction and uncertainty intervals from both the EurOtop 2007 & 2018 non-breaking formulae. Secondly, for cot $\alpha$ = 3.0, the EurOtop 2007 and 2018 curves are very close to each other over the freeboard range 0 to 3.8. The predictions using DHNN lie largely within the 5% confidence limits with an occasional excursion above the upper limit. Our results follow a flatter trend with increasing freeboard showing an increasing divergence from EurOtop as freeboard increases. Thirdly, both EurOtop predictions for cot $\alpha$ = 3.0, the DHNN, our uni-modal and bimodal results are all in close agreement for freeboards in the range from 0.7 to approximately 1.5. The main region of divergence is for freeboards above 1.5. Here, there is evidence of a tendency for the observed overtopping to be larger than expected from current guidance. The trend and preponderance of the observations is above both the upper 5% confidence limit of EurOtop 2018 and the trend of the DHNN predictions. Fourthly, for the case where cot $\alpha$ = 1.5, a divergence between the predictions of Eurotop 2007 and EurOtop 2018 is more obvious for freeboards over approximately 2.0. Our results, both unimodal and bimodal, are well clustered around the EurOtop and DHNN predictions for freeboards less than 2.0. For larger freeboards, our results show large scatter and a trend

and preponderance above both EurOtop and DHNN predictions, with DHNN and EurOtop 2007 providing predictions closer to our results than EurOtop 2018.

In Figs. (5 and 6), the overtopping for bimodal waves spreads beyond the 5% confidence intervals and is more pronounced for values of $R_c/H_{m0} > 2.0$. There is also more vertical scatter in the overtopping rate at lower $R_c/H_{m0}$ for bimodal sea cases than in the unimodal results. Victor and Troch (2012) suggested that for unimodal seas, the scatter values could be due to the influence of wave period. Any such effect would be expected to be amplified in the case of bimodal conditions for which there are a wider range of wave periods; and this is as observed.

*5.3 Wave overtopping of vertical Seawalls*

Results for the vertical seawall are presented in Fig. (7) for both unimodal and bimodal sea conditions. In all the tests considered in this study, the simple wave overtopping formulae for a vertical seawall recommended in EurOtop 2007 & 2018 were used. As in Figs. (5 & 6), unimodal results are shown as red triangles, bimodal results are represented by black diamonds, and DHNN results by blue diamonds. As can be seen from Fig. (7), the unimodal results are mostly within the 5% confidence limits of the EurOtop 2018 formula but the trend with varying freeboard aligns more closely with the EurOtop 2007 formula. In common with our results for the sloping seawall, most of the results for bimodal seas for freeboard > 1.5 are outside the confidence limits of EurOtop 2018. In contrast with the sloping wall cases, in this situation the scatter in observed overtopping does not increase markedly with freeboard. The slope of the trend in overtopping with freeboard matches well with EurOtop 2007, but the preponderance of observations is significantly above the EurOtop 2007 prediction and well above the upper 5% confidence limit of EurOtop 2018.

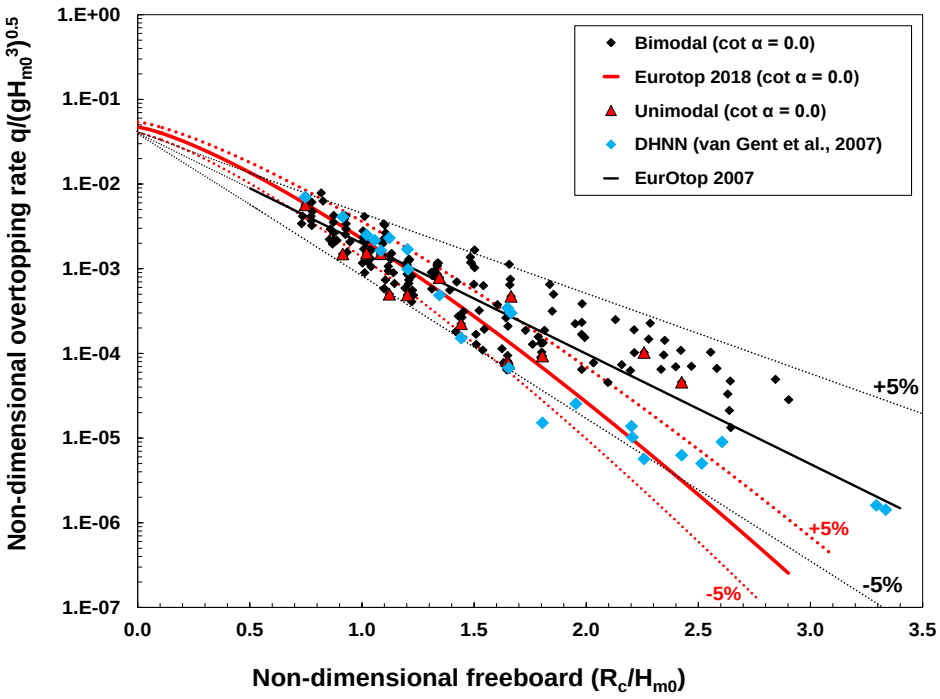


Fig. 7*: Results of non-dimensional overtopping rate against non-dimensional crest freeboard plotted for a vertical seawall with cot α = 0.0*

5.4 Influence of spectral parameters on bimodal waves

From the results presented in the previous section it is clear that the presence of swell can alter the overtopping characteristics. The introduction of swell alters the wave steepness, $S_{m-1,0,}$ and wave period, $T_{m-1,0}$. The values of, and difference between, the peak periods of the wind and swell components are other potential determinands of overtopping. A range of $S_{m-1,0}$ between 0.01 and 0.07 has been tested, and the corresponding surf similarity parameter $\xi_{m-1,0}$ ranges between 2.4 and 5.5. Fig. 8 (a) shows an example of the relationship between wave steepness and different forms of swell in a sea state with *wave height* of 4 metres and peak wind wave period of 7 secs. As suggested in EurOtop 2018, wave steepness reduces with increasing swell percentage, $S_0$, swell peak period and $R^*$ respectively.

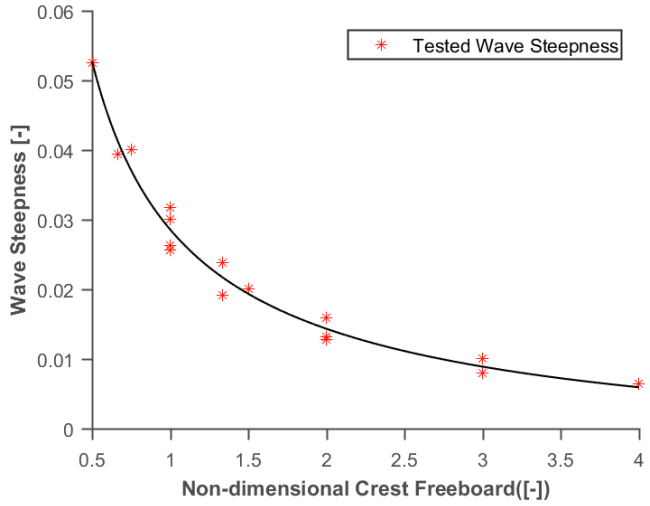


(a)

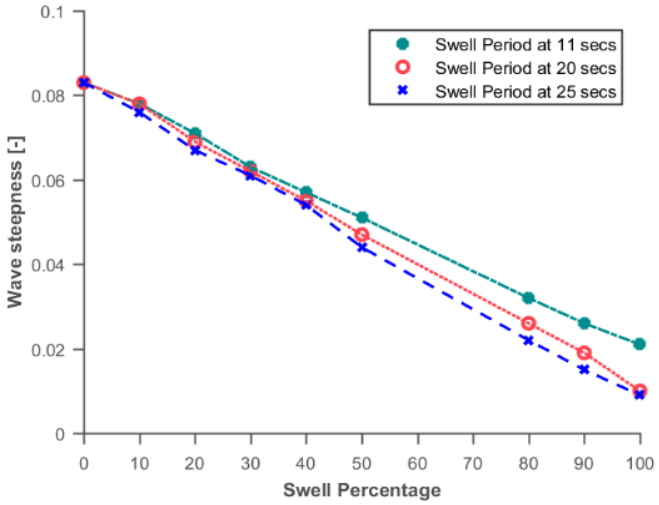


(b)

Figure 8: *(a) Relationship between tested wave steepness and the R*, (b) Variations of wave steepness with swell percentages in a sea state of wave height* of 4 metres and wind wave period of 7 secs *with equal energy but different swell percentages and swell peak periods.*

It is well-known that a higher wave period, (equivalently lower wave steepness) increases overtopping rates, and Eurotop 2018 suggests using $T_{m-1,0}$ to account for the presence of swell as it is weighted towards larger periods; whereas Hawkes et al. (1990) and Kashima et al. (2010) have suggested percentage swell as a useful indicator. In our experiments the correlation between swell percentage and $T_{m-1,0}$ was 0.64, indicating that they represent similar but distinct aspects of the wave conditions. An obscuring factor is that steepness will depend not just on the percentage of swell but also the peak period of the swell, as demonstrated in Fig. (8b). Figures (9a&b) show the non-dimensional overtopping discharges as they vary with $T_{m-1,0}$ and swell percentage respectively. Results corresponding to different wall slopes are shown in red (cot $\alpha$ = 3.0), green (cot $\alpha$ = 1.5) and blue (cot $\alpha$ = 0.). No strong dependence of overtopping on $T_{m-1,0}$ is evident. A slight tendency for overtopping to increase with percentage swell is evident for swell up to 50%, with a slight decrease as swell percentage increases to 75%.

(a)

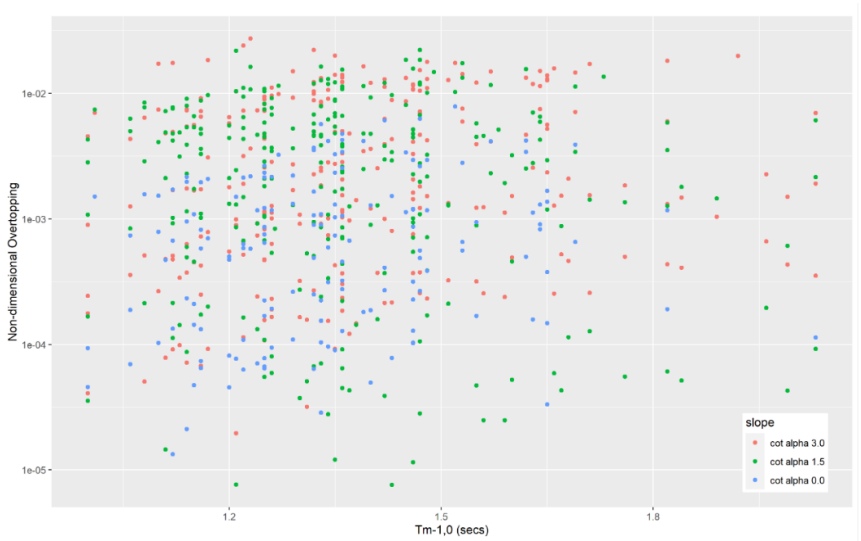


(b)

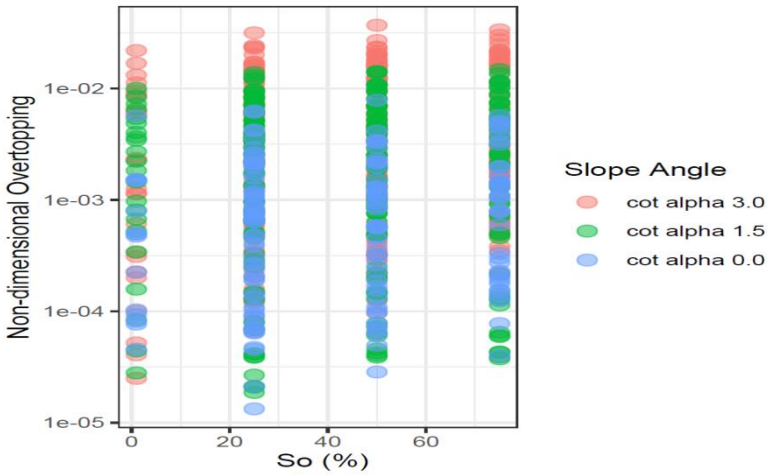


Fig. 9: (a) The relationship between the non-dimensional overtopping rate with $T_{m-1,0}$ and (b) the relationship between non-dimensional overtopping discharge and the swell percentage.

*5.5 Influence of swell percentage*

In each of the sea states investigated, the swell percentage, $S_0$, was varied between 0 (unimodal), 25, 50, and 75%. Fig. 10 shows an expanded form of Fig. 9b to illustrate the influence of $S_0$ on wave overtopping across the three wall slopes.

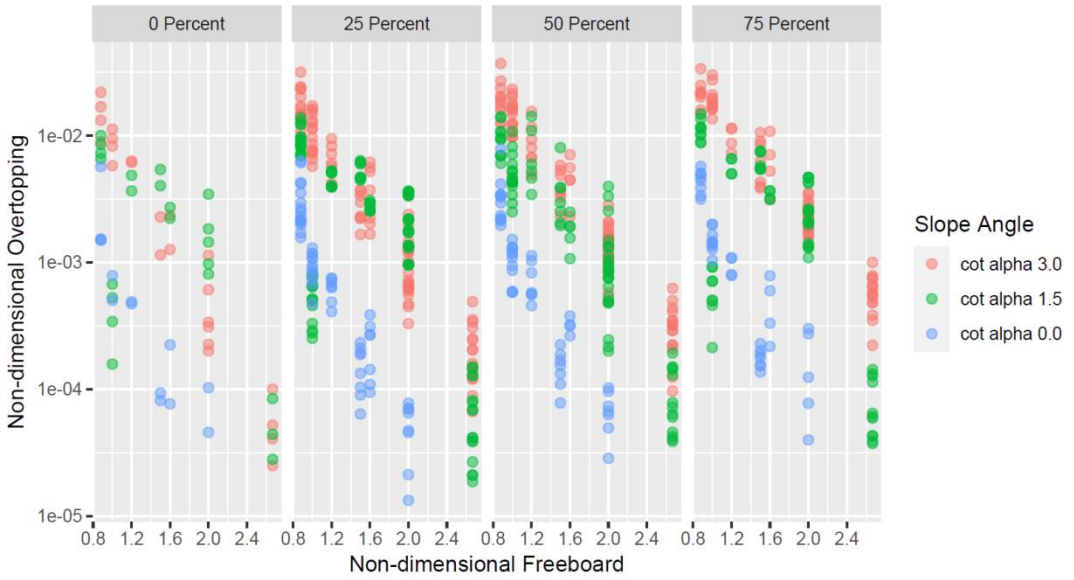


Fig. 10: The relationship between the non-dimensional overtopping rate with freeboard by swell percentages for cot $\alpha$ =0.0 and cot $\alpha$ =1.5 and cot $\alpha$ =3.0.

Several trends are evident in Fig. 10. First, for all swell percentages and all wall slopes the overtopping decreases with freeboard. Second, there is a general trend for overtopping for a fixed freeboard to increase with swell percentages from 0 to 50% and to then level off or decrease slightly as swell percentage increases to 75%. However, there is variation about this pattern across the range of freeboards. Thirdly, comparing the overtopping rates obtained with bimodal seas with those of unimodal seas with equivalent energy content shows that the presence of some (non-zero) level of swell results in an increase in the overtopping discharge. Our finding of the relative insensitivity of overtopping rate to $T_{m-1,0}$ is in agreement with the conclusions of Victor and Troch (2012), van Doorslaer et al., (2015) and EurOtop 2018, that the influence of $T_{m-1,0}$ on overtopping is weak for non-breaking waves.

*5.6 Modified overtopping formula for swell percentages*

The trends in overtopping with respect to seawall slope and $S_0$ suggest the existing formula for overtopping Eq. (2) might be modified to reflect this influence. Four sets of $S_0$ that are considered are 0, 25, 50, and 75 percent, (with 0 percent representing the full wind sea state). Fig 11(a–d) show results obtained by non-linear least squares regression analysis by percentage of swell applied to the observations.

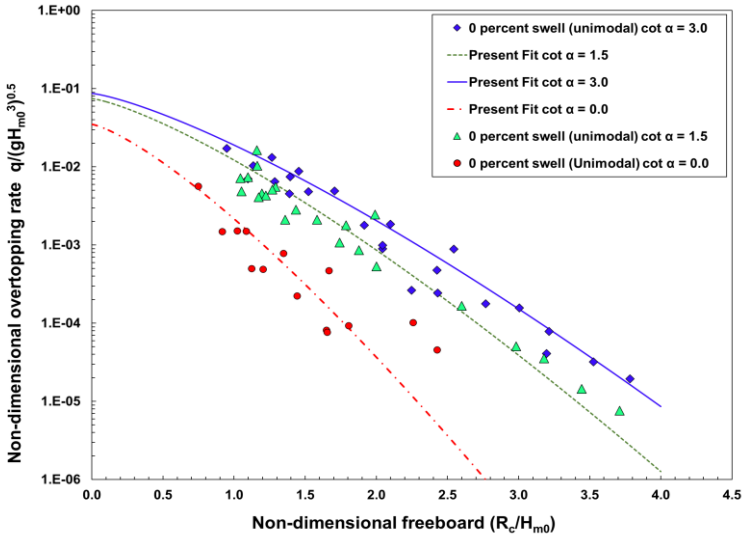


(a)

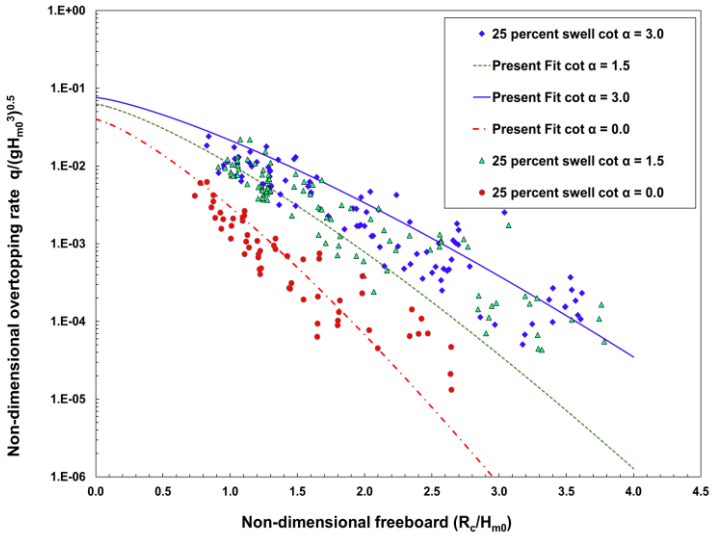


(b)

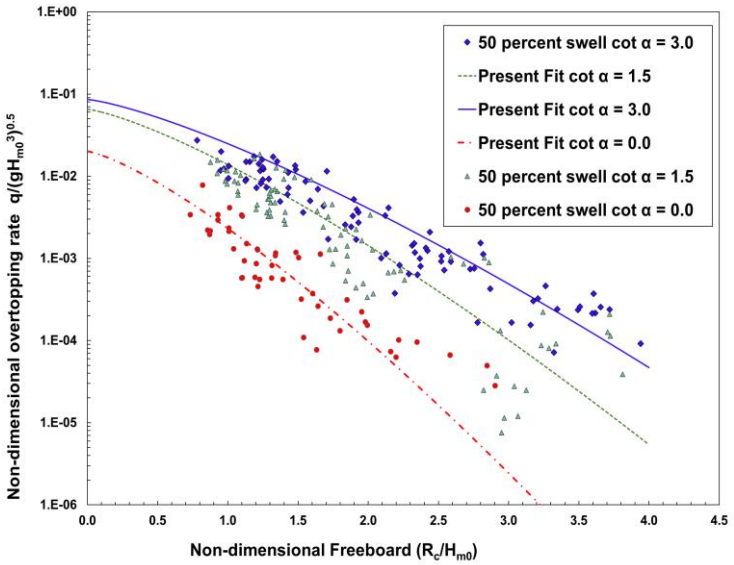


(c)

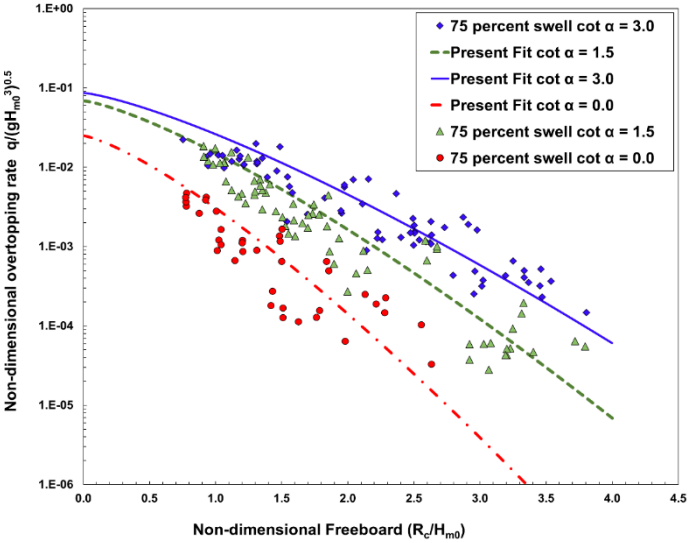


(d)

Fig. 11: *Results of non-linear regression performed on different non-dimensional wave overtopping obtained across three slopes (cot α =1.5, cot α =3.0 and cot α =0.0) for (a) Unimodal seas (0 percent swell), (b) Bimodal seas with 25 percent swell, (c) Bimodal seas with 50 percent swell, and (d) Bimodal seas with 75 percent swell.*

Fig. 12 represent plots of the coefficient values of $A$ and $B$ obtained as a result of the non-linear regression fitted on different percentages of swell obtained across different slopes. The fit for coefficient $B$ has little scatter whereas the fits for coefficient $A$ have wider scatter.

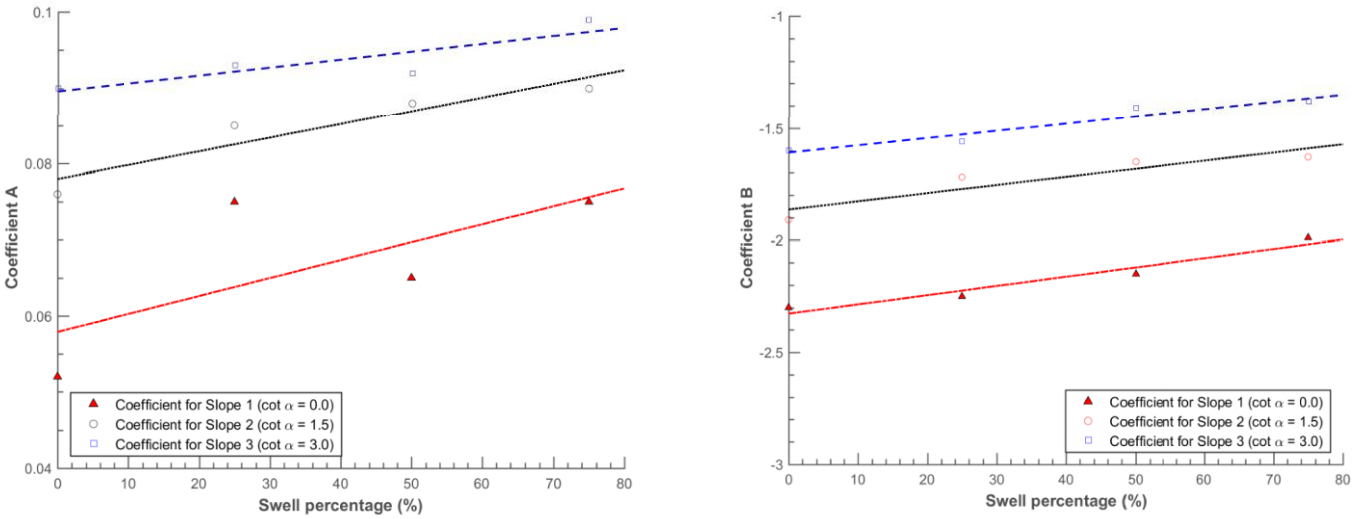


Fig. 12: *(a) Coefficient A as a function of $S_0$, varying from 0 to 75 percent, (b) Coefficient B as a function of $S_0$, varying from 0 to 75 percent,*

The linear variation of $A$ and $B$ with respect to $S_0$ can be expressed as:

$$A_s = A + m_1 S_0 \tag{14a}$$

$$B_s = B + m_2 S_0 \tag{14b}$$

where values of $A_s$ and $B_s$ are the coefficients redefinitions proposed for design formulations under a unidirectionally swell driven bimodal seas. $A$ and $B$ follow the same definition provided in EurOtop 2018 for different impermeable sloping seawalls whose values are dependent on structure slope $cot\alpha$. The constants $m_1$ and $m_2$ are defined by the slope of the lines in Fig. (12). A modified version of Eq. (3) based on the regression against our new observations, which accounts for bimodal conditions may be written as:

$$\frac{q}{\sqrt{gH_{m0}^3}} = A_s . \exp\left( - B_s \frac{R_c}{H_{m0}} \right)^{1.3} \tag{15a}$$

where the values of $A_s$ can be empirically redefined in terms of $S_0$ as:

$$A_s = \begin{cases} A + 0.0002\,S_0 & for \cot\alpha \le 1.5 \\ 0.09 + 0.0001\,S_0 & for \cot\alpha \ge 1.5 \end{cases} \quad (15b)$$

and, for coefficient $B_s$:

$$B_s = \begin{cases} B + 0.0004\,S_0 & for \cot\alpha \le 1.5 \\ -1.609 + 0.0003\,S_0 & for \cot\alpha \ge 1.5 \end{cases} \quad (15c)$$

Eqs. 14(a-c) are defined to cater for the effect of $S_0$ on the overtopping computed for bimodal cases only. The applicability is limited to slopes within the ranges shown ($0 \le \cot\alpha \le 3.0$). The usage also does not contradict the use of Eqs. (3-5) above. Coefficients for different slopes are calculated using the suggestions of Victor and Troch (2012) and van der Meer and Bruce (2013) in Eqs. (3-5), and then determine the equivalent effects due to swell percentage by applying Eqs. 15(a-c). It is because swell percentages follow a linear increasing relationship with the dimensionless overtopping. The trends of this slope are the same for both *cot α = 0* and *cot α = 1.5*. However, there is a significant drift in this case for *cot α ≤ 3.0*. The new formulation presents an improvement to account for the effect of swell percentage in bimodal seas as portrayed by improved RMSE values and bias values of more than 20 percent are obtained respectively across various slopes. Full details of the accuracy assessment can be found in Orimoloye et al., (2020b).

5.7 Assessment of Prediction Accuracy

In this section, the Root Mean Square Errors, (RMSE), and the bias of the errors, (BE), are presented to assess the accuracy provided by the EurOtop (2007 & 2018) formulae. The RMSE can be expressed mathematically as:

$$RMSE = \sqrt{\frac{1}{N_t}.\sum_{n=1}^{N_t}\left(q^*_{pred} - q^*_{measured}\right)^2} \quad (16)$$

where $n$ is test identifier, $N_t$ is the total number of tests under consideration, $q^*_{pred}$ is the predicted dimensionless overtopping, and $q^*_{measured}$ is the measured dimensionless overtopping values. The bias of the measurement is defined in terms of the average of the overall dispersion of individual values of $q^*_{pred}$ and the $q^*_{measured}$

$$BIAS = \frac{1}{N_t}.\sum_{n=1}^{N_t}\left(q^*_{pred} - q^*_{measured}\right) \quad (17)$$

and is a measure of systematic over- or under-prediction.

Table 4 summarises the RMSE and bias of the two EurOtop formulae and our proposed formula for the non-dimensional overtopping under unimodal and bimodal conditions for the three wall slopes.

Table 4. RMSE and bias of EurOtop (2007), EurOtop (2018) and Equation (15a-c) against observations.

| **Formulation** | **EurOtop (2007)** | | **EurOtop (2018)** | | **Equation (16)** | |
|---|---|---|---|---|---|---|
| **Parameter** | **RMSE** | **Bias** | **RMSE** | **Bias** | **RMSE** | **Bias** |
| All tests ($cot\ \alpha = 3.0$) | 0.002964 | 6.96E-06 | 0.003652 | 7.46E-06 | 0.00271 | 6.10E-06 |
| Unimodal | 0.002365 | 7.99E-04 | 0.002838 | 8.83E-04 | 0.002214 | 6.34E-04 |
| Bimodal | 0.004011 | -6.38E-05 | 0.004634 | -7.41E-05 | 0.003758 | -4.95E-05 |
| All tests ($cot\ \alpha = 1.5$) | 0.003076 | -1.63E-03 | 0.003362 | -1.69E-03 | 0.002595 | -1.36E-03 |
| Unimodal | 0.001745 | 1.31E-04 | 0.001906 | 1.36E-04 | 0.001355 | 1.06E-04 |
| Bimodal | 0.002488 | -4.52E-04 | 0.003038 | -5.18E-04 | 0.002279 | -3.78E-04 |
| All tests ($cot\ \alpha = 0.0$) | 0.008912 | 3.64E-04 | 0.009724 | 3.84E-04 | 0.006087 | 2.84E-04 |
| Unimodal | 0.000941 | 5.30E-04 | 0.001029 | 5.80E-04 | 0.000792 | 4.58E-04 |
| Bimodal | 0.008298 | 3.54E-04 | 0.009668 | 3.65E-04 | 0.006284 | 3.22E-04 |

In all cases the Eurotop (2007) has smaller RMSE than the EurOtop 2018 formula, being of the order of 10% less. This is within the guideline maximum benchmark allowance of 27% stipulated in EurOtop 2018. Our proposed formula provides an improvement on the EurOtop 2007 formula in all cases. Errors and bias in all the formulae are smallest for the unimodal case, with RMSE being a factor of 2 to 10 times larger for bimodal cases than in the respective unimodal cases.

As may be inferred from Figures (5-7) our experimental results lie above those predicted by EurOtop 2007 and 2018 formulae. The modification to the EurOtop 2018 we have proposed also lies above the predictions made with EurOtop 2007 and 2018 formulae. To illustrate the effects and relative performances we have plotted a set of curves for wall slope cot$\alpha$ =3.0 in Fig. 13. Observations for unimodal and bimodal cases are shown as red triangles and black diamonds respectively. Predictions made with DHNN are shown as blue diamonds. Predictions and confidence limits for EurOtop 2007, EurOtop 2018 (using $T_{m-1,0}$) and Equation 15 are shown in red, black and green lines respectively.

In our experiments the geometry of the seawall clearly has an influence on the variation of overtopping with the swell wave content of the wave conditions. The relative performance of EurOtop 2007 and EurOtop 2018 formulae is unexpected and we hypothesise that at least some of the increase in overtopping is due to the longer period waves causing a temporary reduction in freeboard, during which period shorter period waves can ‘ride up’ and cause greater overtopping than might otherwise be expected. That is, the phase relationship between individual long and short period waves may play an important role. Both the width of the spectral peaks, (swell and

wind sea), and their separation are likely to control such a mechanism which, for its importance, will depend critically upon the frequency of occurrence of the necessary phasing between shorter and longer wave components.

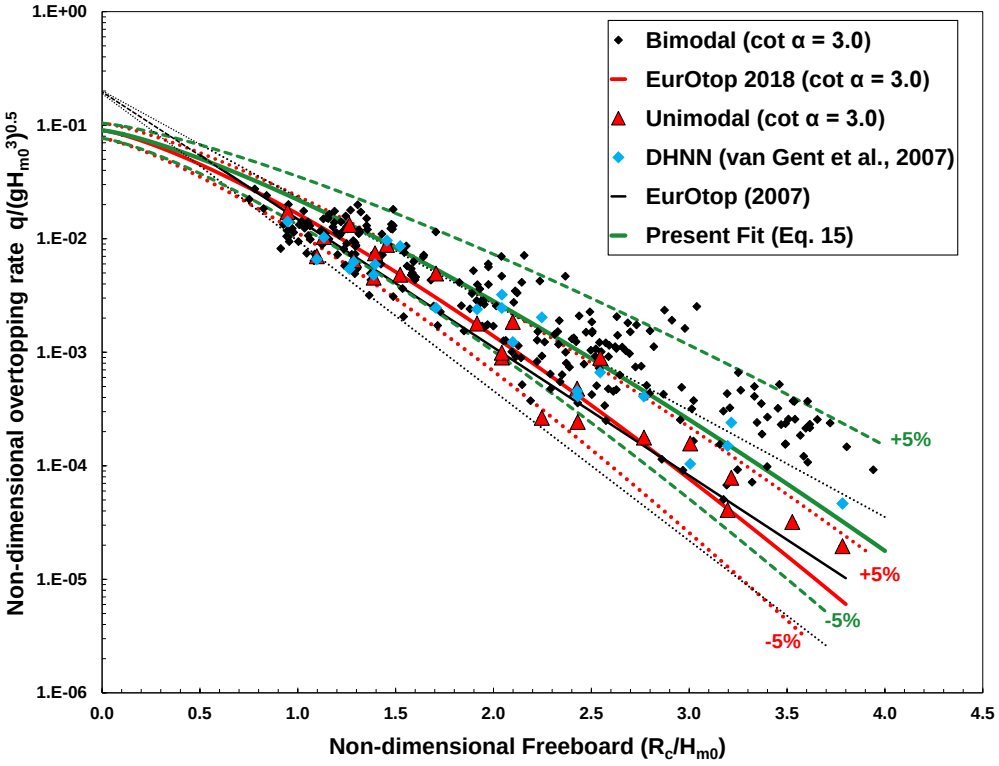


Fig. 13: *Results showing the predicted non-dimensional overtopping rate against the non-dimensional crest freeboard presented by the present fit as indicated in Equation (15) the sloping wall with cot α =3.0*

## 6. **Conclusions**

In this paper, a systematic set of wave overtopping tests have been conducted on impermeable seawalls facing bimodal sea conditions in a wave flume. The tests are based on the concept of a conserved energy spectrum in which the energy of the sea state is held constant while the shape of the spectrum is varied across unimodal to bimodal forms permitting different percentages of swell to be introduced. Tests were conducted for non-breaking waves impinging upon three different wall slopes, including a vertical wall.

The results show that for given wave conditions overtopping decreases with wall slope (least with vertical walls and most with mild sloping walls). Unimodal overtopping results agree very well with current guidance. Bimodal results, using the wave period $T_{m-1,0}$, agree well with current guidance for non-dimensional freeboards in the range between approximately 0.8 and 1.5. Overtopping rates under bimodal conditions diverge from current guidance as the freeboard exceeds 1.5. The effect is most noticeable for the mildest seawall slope but in all cases both the trend and the preponderance of observations was underestimated by current guidance and above the upper 5% confidence limits proposed by EurOtop 2018. The trend in overtopping with freeboard was in better alignment with the formula proposed in EurOtop 2007 but the preponderance of results were also above the EurOtop 2007 predictions. Overtopping under bimodal conditions showed little relationship to wave period and some dependence upon swell percentage. Again, this was strongest for the milder slopes. The results have been used to develop a simple modification to the EurOtop 2018 guidance for bimodal conditions based on the percentage of swell.

While the introduction of swell clearly leads to an increase in overtopping in comparison to purely unimodal wave conditions the mechanisms responsible for this remain unclear. Our results suggest that relating it solely to reducing the mean wave steepness is over simplistic. Similarly, the dependence of overtopping with swell percentage is not a monotonic relationship. We have found that swell percentage has a stronger influence on overtopping than $T_{m-1,0}$.

The strength of the effect of bimodality on overtopping varies with the geometry of the seawall and we surmise that this is likely to be linked to the phase relationship between long and short wave components of the combined wave conditions. Our results relate most to locations at which swell, and wind sea waves have similar directions. They indicate that in situations where bimodal wave conditions exist overtopping may exceed that expected from design guidance based on unimodal conditions.

**Acknowledgements**
This research was funded by The Petroleum Technology Trust Fund (PTDF), Nigeria (Grants No. OSS/PHD/842/16). The authors would like to acknowledge Thomas van Veelen for his assistance while conducting the experimental tests. The authors also acknowledge Thomas Lykke Andersen and Peter Frigaard for the generous workshop on the generation and analysis of waves in physical models as well as useful discussions with both Alison Raby and William Allsop during their respective visits to the Swansea University Coastal Engineering Flume.

## References


Bradbury, A., Mason, T., Poate, T., 2007. Implications of the spectral shape of wave conditions for engineering design and coastal hazard assessment–evidence from the English Channel. 10th International Workshop on Wave Hindcasting and Forecasting and Coastal Hazard Symposium North Shore, Oahu, Hawaii, November, 11–16.

Burcharth, H., Hughes, S., 2002. Part vi, design of coastal project elements. Coastal Engineering Manual; US Army Corps of Engineers: Washington, DC, USA.

Burcharth, H. F., Andersen, T. L., 2007. Overtopping of rubble mound breakwaters with front reservoir. Coastal Engineering 2006: (In 5 Volumes), p4605–4615.

Chen. W., van Gent, M.R.A., Warmink, J.J., Hulscher, S.J.M.H., 2020. The influence of a berm and roughness on the wave overtopping at dikes, *Coastal Engineering*, 156, https://doi.org/10.1016/j.coastaleng.2019.103613,

Clarke, J. Hr DAQ Data acquisition and analysis. IT632 Software Manual 2010, 52 pages.

De Waal, J. P. and van der Meer, J. W., 1993. Wave runup and overtopping on coastal structures. Coastal Engineering, p1758–1771.

Den Bieman J.P., Wilms J.M., Van den Boogaard H.F.P., Van Gent M.R.A., 2020. Prediction of Mean Wave Overtopping Discharge Using Gradient Boosting Decision Trees, *Water*, 12, 1703; doi:10.3390/w12061703

Ewans, K. C., Bitner-Gregersen, E. M., Soares, C. G., 2006. Estimation of Wind Sea and Swell Components in a Bimodal Sea State. Journal of Offshore Mechanics and Arctic Engineering, p128-265.

Franco, L., de Gerloni, M., der Meer, J. V., 1994. Wave overtopping on vertical and composite breakwaters. Proceedings from 24th International Conference on Coastal Engineering Kobe, ASCE, New York.

Franco, L., Geeraerts, J., Briganti, R., Willems, M., Bellotti, G., De Rouck, J. D., 2009. Prototype measurements and small-scale model tests of wave overtopping at shallow rubble-mound breakwaters: the Ostia-Rome yacht harbour case. Coastal Engineering 56 (2), p154–165.

Gallach Sanchez, D., Illegems, M., Willems, Y., Troch, P., Kortenhaus, A., 2016. Experimental study of average overtopping performance on steep low-crested structures for shallow water conditions. Coastlab 2016, p1–10.

Goda, Y., 2010. Random Seas and Design of Maritime Structures. World Scientific Publishing Co. Pte. Ltd.

Hanson, J. L., Phillips, O. M., 2001. Automated analysis of ocean surface directional wave spectra. Journal of Atmospheric and Oceanic Technology, 18 (2), p277–293.

Hasselmann, K., Barnett, T. P., Bouws, E., Carlson, H., Cartwright, D. E., Enke, K., Ewing, J. A., Gienapp, H., Hasselmann, D. E., Kruseman, P., Meerburg, A., Muller, P., Olbers, D. J., Ritcher, K., Sell, W., Walden, H., 1973. Measurements of wind-wave growth and swell decay during the Joint North Sea Wave Project (JONSWAP). Dtsch. Hydrogr A8 (12).

Hawkes, P. J., Coates, T., Jones, R. J., 1998. Impacts of Bimodal Seas on Beaches, Hydraulic Research Wallingford. HR Wallingford Report, 80.

Hedges, T., Reis, M., 1998. Random wave overtopping of simple sea walls: a new regression model. Proceedings of the Institution of Civil Engineers, 130 (1), p1–10.

Hedges, T., Shareef, M., 2003. Predicting seawall overtopping by bimodal seas. Coastal Engineering 2002: Solving Coastal Conundrums, p2153–2164.

Kashima, H., Hirayama, K., Hasegawa, I., 2010. Experimental study on wave overtopping rate of long period swell on seawall. Journal of Japan Society of Civil Engineers, Ser B2 66 (1), p716–720.

Kortenhaus, A., Oumeraci, H., Geeraerts, J., De De Rouck, J., Medina, J., Gonźlez-Escrivá, J., 2004. Laboratory effects and other uncertainties in wave overtopping measurements. In: Book of Abstracts 29th ICCE. pp. p343–343.

Mansard, E. P., Funke, E. R., 1980. The measurement of incident and reflected spectra using a least squares method. Proceedings 17th ICCE, Sydney, p154–172.

Mason, T.; Pullen, T.; Powell, K. Hydraulics Research Merlin wave generation programme. RT007 Software Manual 2014, 73 pages

Orimoloye, S., Karunarathna, H., Reeve, D. E., 2019a. Effects of swell on wave height distribution of energy conserved bimodal seas. Journal of Marine Science and Engineering 7 (3), 79. https://doi.org/10.3390/jmse7030079

Orimoloye, S., Horrillo-Caraballo, J., Karunarathna, H., and Reeve, D. E., 2019b. Modelling wave overtopping of steep impermeable structures under bimodal sea conditions", In Proceedings of the 8th International Conference of Coastal Structures, Hannover, Germany, https://doi.org/10.18451/978-3-939230-64-9_121.

Orimoloye, S., Karunarathna, H., Reeve, D.E., 2020a. Reflection Analysis of Impermeable Slopes under Bimodal Sea Conditions. J. Mar. Sci. Eng., 8, p133, https://doi.org/10.3390/jmse8020133

Orimoloye, S., Horrillo-Caraballo, J., Karunarathna, H., and Reeve, D. E., 2020b. "A novel method for wave overtopping study under bimodal sea conditions". (Submitted to MethodX).

Owen, 1980. Design of seawalls allowing for wave overtopping. HR Wallingford Technical Report EX924, UK.

Owen, M., 1982. Overtopping of sea defences. Proceedings from Conference Hydraulic Modelling of Civil Engineering Structures BHRA University of Warwick Coventry, p469–480.

Pullen, T., Allsop, N., Bruce, T., Kortenhaus, A., Schüttrumpf, H., van der Meer, J., 2007. EurOtop. Wave overtopping of sea defences and related structures: assessment manual, 178.

Reeve, D.E., Chadwick, A., Fleming, C., 2015. Coastal Engineering: Processes, Theory and Design Practice. Third Edition, CRC Press, Taylor & Francis Group, London.

De Rouck, J. D., Verhaeghe, H., Geeraerts, J., 2009. Crest level assessment of coastal structures — General overview. Coastal Engineering 56 (2), p99–107.

Rychlik, I., Johannesson, P., Leadbutter, M. R., 1997. Modelling and Statistical Analysis of Ocean-wave Data Using Transformed Gaussian Processes. Marine Structures 10, 13–47.

Schaeffer, H. A., 1996. Second-order wavemaker theory for irregular waves. Ocean Engineering 23 (1), 47–88.

Smith, G. M., Seijffert, J. W. W., and van der Meer, J. W., 1995. Erosion and overtopping of a grass dike large scale model tests. Coastal Engineering, p2639–2652.

Thompson, D., Karunarathna, H.K., Reeve, D.E., 2017. Modelling extreme wave overtopping at Aberystwyth promenade. Water 9 (9), p663-678.

Troch, P., Geeraerts, J., van de Walle, B., De De Rouck, J., van Damme, L., Allsop, W., Franco, L., 2004. Fullscale wave-overtopping measurements on the Zeebrugge rubble mound breakwater. Coastal Engineering 51 (7), p609–628.

van der Meer, J.W., 1993. Conceptual design of rubble mound breakwaters, Publication 483, WL, Delft Hydraulics, Delft.

van der Meer, J.W., 1995. Wave run-up and wave overtopping at dikes. Journal of Waterway, Port, Coastal, and Ocean Engineering.

van der Meer, J., Bruce, T., 2013. New physical insights and design formulas on wave overtopping at sloping and vertical structures. Journal of Waterway, Port, Coastal, and Ocean Engineering, 140 (6), 04014025.

van der Meer, J.W., Verhaeghe, H., Steendam, G., 2005. Database on wave overtopping at coastal structures. CLASH WP2 database, Inframm, Marknesse, NL.

van der Meer, J.W., Verhaeghe, H., Steendam, G. J., 2009. The new wave overtopping database for coastal structures. Coastal Engineering, 56 (2), p108–120.

van der Meer, J.W., Allsop, W.N., Bruce, T., De De Rouck, J., Kortenhaus, A., Pullen, T., Schüttrumpf, H., Troch, P., Zanuttigh, B., 2018. Manual on wave overtopping of sea defences and related structures. EurOtop Manual.

van der Werf, I., Van Ghent, M.R.A., 2018. Wave overtopping over coastal structures with oblique wind and swell waves. Journal of Marine Science and Engineering, 6 (4), p149.

van Doorslaer, K., De Rouck, J., Audenaert, S. and Duquet, V., 2015. Crest modifications to reduce wave overtopping of non-breaking waves over a smooth dike slope. *Coastal Engineering*, *101*, pp.69-88.

Van Gent, M.R.A., 1994. The modelling of wave action on and in coastal structures, Coastal Engineering, 22 (3-4), p311–339.

Van Gent, M.R.A. (2001), Wave run-up on dikes with shallow foreshores, ASCE, Journal of Waterways, Port, Coastal and Ocean Engineering, September/October 2001 issue. Vol. 127, No 5 p254-262.

Van Gent, M.R.A. (2002), Coastal flooding initiated Van Gent, M.R., van den Boogaard, H.F., Pozueta, B. and Medina, J.R., 2007. Neural network modelling of wave overtopping at coastal structures. *Coastal Engineering*, *54*(8), p586-593.

Van Gent, M.R.A., Smith, G., 1999. Physical model investigations on coastal structures with shallow foreshores: 2D model tests with single and double-peaked wave energy spectra. Hydraulic Lab. report, Number, V257(235182), 70 pages.

Van Gent, M.R.A. and Van der Werf, I., 2019. Influence of oblique wave attack on wave overtopping and wave forces on rubble mound breakwater crest walls, *Coastal Engineering*, 151, 78-96, https://doi.org/10.1016/j.coastaleng.2019.04.001.

Victor, L., Troch, P., 2012. Wave overtopping at smooth impermeable steep slopes with low crest freeboards. Journal of Waterway, Port, Coastal, and Ocean Engineering, 138 (5), p372–385.

Zelt, J. A., Skjelbreia, J. E., 1992. Estimating incident and reflected wave fields using an arbitrary number of wave gauges. Proceedings, 23rd ICCE, Venice, p777–788.